A Comparison of Two Approaches for Adaptive Sampling of Environmental Processes Using Autonomous Underwater Vehicles

Christopher J. Cannell, Daniel J. Stilwell

The Bradley Department of Electrical and Computer Engineering
Virginia Polytechnic Institute and State University
Blacksburg, VA 24061
{*ccannell, stilwell*}*@vt.edu*

Abstract— **Two classes of adaptive sampling of underwater processes are considered for autonomous underwater vehicle (AUV) applications. The first approach is based on estimating parameters of an assumed process model using either Kalman filter or least squares techniques. The second, nonparametric approach is based on information-theoretic concepts and incorporates a classification phase in lieu of a process model. Two applications of each method are evaluated for processes with closed boundaries. Specifically, we utilize a finite element simulation of neutral tracer injection advected by a turbulent flow field.**

I. Introduction

Adaptive sampling algorithms enable one or more AUVs to determine optimal routes, locations, and times to collect scientific measurements in response to real-time environmental measurements. A key feature of these algorithms is that sampling strategies continuously adapt in response to real-time environmental measurements without human intervention.

In this investigation, two adaptive sampling approaches are used for modeling and tracking a marine process. The first technique is a model-based method in which parameters of an assumed model are estimated using either nonlinear least squares or a Kalman filter. The second technique is a nonparametric approach for which an information theoretic methodology is utilized which does not require an explicitly defined process model.

For the parametric approach, two methods for estimating the unknown parameters of the process model are considered. The first method is related to standard self-localization and mapping algorithms where the unknown parameters in an assumed measurement model are states in a Kalman (or information) filter. An example is presented where the unknown parameters correspond to the mean and variance of a two dimensional scaled Gaussian distribution which is utilized to model the dispersal of a neutral tracer in an ambient flow. Using this method, the AUV estimates the unknown parameters of the measurement model while minimizing the state error covariance. In the second method, nonlinear least squares regression is used to fit the parameters of an elliptical measurement model to the boundary of the same process.

The nonparametric approach utilizes an information theory based algorithm, developed in [1], which characterizes the boundary of a closed process via sequential classification and tracking phases. During the classification phase, measurements are collected in the assumed ambient flow and an empirical distribution is formed. This distribution represents the measurements taken outside the process. As the AUV collects new measurement sets, updated empirical distributions are computed and compared to the assumed ambient distribution using the minimum description length (MDL) test. This test utilizes the Kullback-Leibler divergence, also known as relative entropy, to determine if two distributions are different in a statistically significant manner. This result is then used as a test for identifying data that is statistically different from the ambient distribution. The transition to a statistically different distribution is assumed to correspond to the entry into the interior of the feature of interest – in our case, a neutral tracer patch.

Simulations are performed using the Virginia Tech Adaptive Sampling Simulator [2]. For the work presented, only static data sets are considered that are derived from finite element simulations of neutral tracer injections in a turbulent flow field.

Other research that is focused on mapping airborne plumes has utilized a spatial model of the plume based on the underlying dispersion physics [3], [4], [5]. The utility of these parametric approaches for small-scale underwater applications is not clear, since underwater plumes are dominated by turbulence and filament-based transport that are not easily captured by spatial models. In [6], parameter estimation using an extended Kalman filter is

reported in which the process model is a linear surface. Although the utility of a linear surface model might be limited, it enables closed-form computation of AUV trajectories that locally maximize information gain.

A number of strategies for nonparametric adaptive sampling are found in the literature, though the application is typically plume source localization. For airborne applications, examples include [7] where mobile robots navigated upwind to find a plume source whenever a binary odor sensor indicated the presence of the plume. For underwater applications, examples include [8], where a robotic lobster continuously moved two antenna, creating a local spatial average to estimate the direction of the plume source. Other examples include [9], [10], in which plume source localization algorithms are presented along with experiments in which a REMUS AUV successfully locates the source of an underwater plume.

II. Parametric Approach

A. Extended Kalman Filter

An Extended Kalman Filter [11] is utilized to estimate unknown parameters of a scaled multivariate Gaussian measurement model. Let $x(k) \in \mathbb{R}^3$ represent the 2-D position and heading of the AUV at time $k = \{1, 2, ...\}$. A planar kinematic model is assumed for the AUV dynamics given by the discrete difference equation

$$\begin{aligned} x(k+1) &= f(x(k), u(k)) + w(k) \\ z(k) &= h(x(k)) + v(k) \end{aligned} \tag{1}$$

where

$$f(x(k), u(k)) = \begin{bmatrix} x_1(k) + u_1(k)\cos(x_3(k))\,h \\ x_2(k) + u_1(k)\sin(x_3(k))\,h \\ x_3(k) + u_2(k)h \end{bmatrix} \tag{2}$$

The state vector $x(k) = [x_1(k), x_2(k), x_3(k)]^T$ is composed of Cartesian position $[x_1(k), x_2(k)]^T$ and heading $x_3(k)$. The vector $u(k) = [u_1(k), u_2(k)]^T$ is composed of linear velocity $u_1(k)$ and angular velocity $u_2(k)$. The iteration time step is the scalar h.

The noise vectors $w(k) \in \mathbb{R}^3$ and $v(k) \in \mathbb{R}^p$ are independent identically distributed Gaussian random variables with distributions $P(w) \sim N(0, Q)$ and $P(v) \sim N(0, R)$, respectively.

The estimates for $x(k)$ and $z(k)$ are

$$\begin{aligned} \hat{x}(k+1|k) &= f(\hat{x}(k|k), u(k)) \\ \hat{z}(k+1|k) &= h(\hat{x}(k+1|k)) \end{aligned} \tag{3}$$

where $\hat{x}(i|j)$ is the estimate of $x(i)$ given $\{u(j), u(j-1), ..., u(0)\}$ and $\{y(j), y(j-1), ..., y(0)\}$. Likewise, $\hat{z}(i|j)$ is the estimate of $z(i)$ given $\hat{x}(i|j)$.

An extended Kalman Filter requires the Jacobians

$$\begin{aligned} A(k) &= \frac{\partial f}{\partial x}(\hat{x}(k|k), u(k)) \\ H(k) &= \frac{\partial h}{\partial x}(\hat{x}(k|k-1)) \end{aligned} \tag{4}$$

The Joseph's form [12] of the covariance update equation is used in lieu of the standard update equation. The use of the Joseph's form provides a more numerically robust calculation of the covariance matrix which preserves symmetry at the cost of additional computation.

$$\begin{aligned} P(k|k) = (I - K(k)H(k))\,P(k|k-1)\,(I - K(k)H(k))^T \\ + K(k)RK^T(k) \end{aligned} \tag{5}$$

B. Parameter Estimation of a Scaled Multivariate Gaussian Field

The extended Kalman Filter can be used to estimate the parameters of a measurement model representing the process being measured. Parameters of the measured process are augmented to the AUV states and estimated as states in an extended Kalman filter. The scaled Gaussian measurement model is chosen as

$$\phi(k) e^{-\left\{\frac{1}{2}(p(k)-m(k))^T C(k)^{-1}(p(k)-m(k))\right\}} \tag{6}$$

where $\phi(k)$ is a scaling term, $C(k) = \begin{bmatrix} c_1(k) & 0 \\ 0 & c_2(k) \end{bmatrix}$ is the covariance matrix, $p(k) = [x_1(k), x_2(k)]^T$, and $m(k) = [m_1(k), m_2(k)]^T$ is the mean in the x_1 and x_2 directions respectively.

The parameters of the measurement model,

$$s(k) = [m_1(k), c_1(k), m_2(k), c_2(k), \phi(k)]^T \tag{7}$$

are augmented to the planar AUV kinematics as

$$\begin{bmatrix} x(k+1) \\ s(k+1) \end{bmatrix} = \begin{bmatrix} f(x(k), u(k)) \\ s(k) \end{bmatrix} + w_s(k) \tag{8}$$

The AUV measurement is composed of a scalar environmental measurement and the AUV's position.

$$\begin{aligned} z_s(k) = \begin{bmatrix} \phi(k) e^{-\left\{\frac{1}{2}(p(k)-m(k))^T C(k)^{-1}(p(k)-m(k))\right\}} \\ x_1(k) \\ x_2(k) \end{bmatrix} \\ + v_s(k) \end{aligned} \tag{9}$$

Simulations are conducted using the data shown in Figure 1. The AUV is programmed to survey the area of interest using the track lines shown in Figure 2. Using the Extended Kalman Filter estimation algorithm the parameters estimated produced the scaled Gaussian distribution shown in Figure 3.

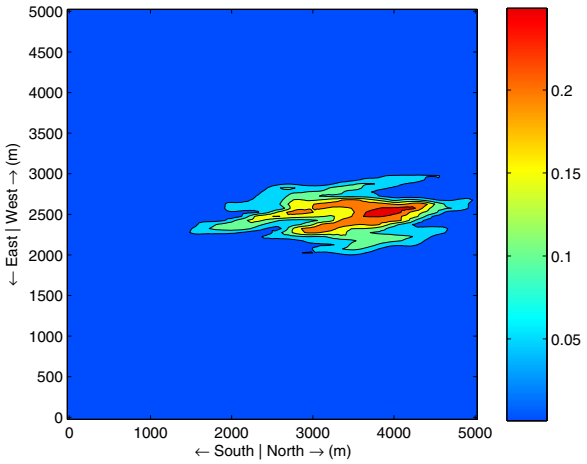

Fig. 1. Neutral tracer advected by a turbulent flow field.

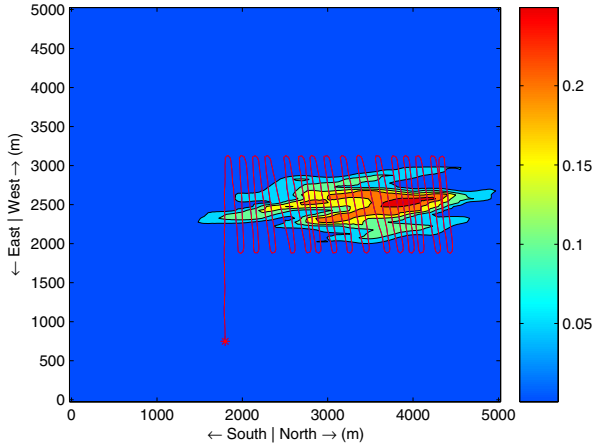

Fig. 2. True and estimated vehicle trajectories estimating a neutral tracer. The AUV runs preprogrammed track lines through the field.

C. Least Squares Regression for an Ellipse

In this section, we consider the parametric approach of fitting the ellipse model defined by

$$\frac{(x_1(k)-h)^2}{a^2}+\frac{(x_2(k)-\kappa)^2}{b^2}=1 \tag{10}$$

to the boundary of a neutral tracer measured by an AUV. A nonlinear least squares algorithm [13] is used to identify the unknown parameters in (10). The known vector $x(k)$ corresponds to the Cartesian position of the vehicle $[x_1(k), x_2(k)]^T$ while $\lambda = [h, \kappa, a, b]^T$ are the unknown parameters. The parameters h and κ represent the offset of the ellipse in the x_1 and x_2 axis, while a and b represent the semimajor and semiminor axis lengths of the ellipse.

As with the scaled multivariate Gaussian parameter estimation problem, the parameters of the ellipse are assumed to be constant. The vehicle is programmed to run track lines over the domain as shown in Figure 4. A measurement is taken when the vehicle passes the neutral tracer boundary, according to

$$\begin{aligned} z(k) > \alpha \quad &\text{and} \quad z(k-1) < \alpha \\ &\text{or} \\ z(k) < \alpha \quad &\text{and} \quad z(k-1) > \alpha \end{aligned}$$

where α is a predefined threshold. The measurement, $z(k)$ corresponds to the equation

$$z(k) = \frac{(x_1(k)-h)^2}{a^2}+\frac{(x_2(k)-\kappa)^2}{b^2} \tag{11}$$

Before the measurement is used, it is scaled according to $y(k) = \frac{z(k)}{\alpha}$ in order to match the ellipse equation (10). As the AUV traverses the neutral tracer new measurements are collected along the process boundary depicted by the blue circles in Figure 4. With each new measurement, nonlinear least squares can be used to estimate the unknown ellipse parameters based on all past measurements. The dashed red ellipse in Figure 4 represents the resultant ellipse estimated using nonlinear least squares based on all boundary measurements taken by the vehicle. To provide a ground truth, nonlinear least squares was performed using the set of all boundary points contained in the neutral tracer data set. The resultant ellipse depicted as a dotted yellow line in Figure 4 represents the mean square error best fit.

The AUV samples a small cross section of the neutral tracer as shown by the solid black line in Figure 4. Based on the sample points taken by the vehicle an estimate of the ellipse parameters is made which can be used to determine path planning for the remainder of the neutral tracer. Figure 5 shows the ellipse parameter errors versus number of sampling points taken. The initial conditions

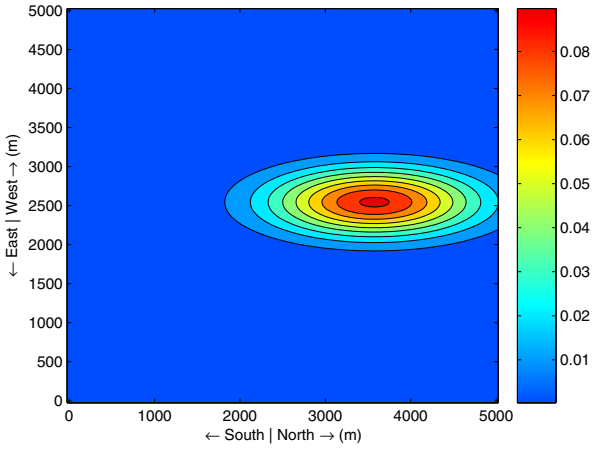

Fig. 3. Estimated Gaussian distribution of the neutral tracer using alternate Gaussian parameter estimation algorithm.

are shown at sampling point zero. The first update occurs at the fourth sampling point and updates continue for every sampling point thereafter.

A drawback of this approach is that convergence of the unknown parameters to a meaningful result is not guaranteed. Initial conditions must be chosen sufficiently close to their true values in order for the unknown parameters to converge.

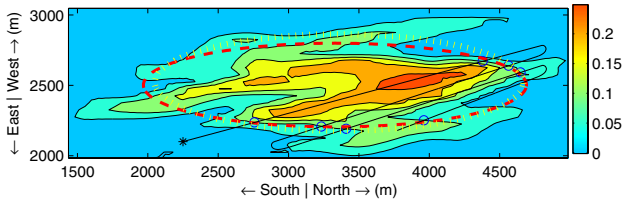

Fig. 4. Simulation results from an AUV measuring the boundary of a neutral tracer. The AUV runs preprogrammed track lines through the field shown by the solid black line. The blue circles indicate where measurements of the tracer boundary were taken. The dashed red line corresponds to the estimated ellipse. As a ground truth nonlinear regression was performed using all 0.1 boundary points in the data set which resulted in the dotted yellow ellipse.

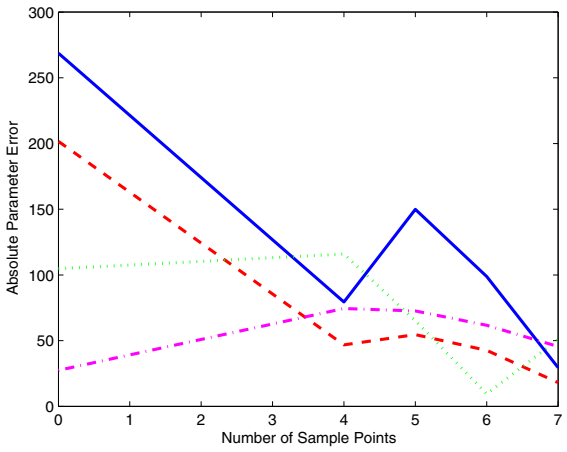

Fig. 5. Ellipse parameter estimation errors corresponding to each sampling point. The parameters h and κ are the solid blue and dashed red lines, respectively. The parameters, a and b, are the dotted green and dash-dot magenta lines, respectively. The parameter errors at sampling point zero denote the initial conditions with updates occurring at sampling points four and beyond.

D. Discussion of Parametric Adaptive Sampling

For the neutral tracer patch, the parametric adaptive sampling algorithms considered herein display shortcomings that may limit their utility for sampling small-scale underwater processes. Of particular concern is the availability of models that adequately represent small-scale marine processes. While the two models considered in Section II display acceptable results for the neutral tracer patch, our experience suggests that changes to vehicle trajectory (and measured data) and initial conditions can lead to instability in the model estimation process. Overall, we find that parametric approaches based on an extended Kalman (or information) filter provide disappointing results, and suggest the need to investigate nonparametric approaches to adaptive sampling.

III. Nonparametric Approach

A. Boundary Detection

The information theoretic techniques presented in [1] provide a means of detecting boundaries between statistically distinct regions. The ideas in sections III-A and III-B were developed in [1], [14] and [15].

In the nonparametric approach, distinct regions are classified using learned empirical distributions representing the governing probability laws. Once the classification phase identifies two distinct regions, their respective empirical distributions can be used to discern in which region a vehicle resides.

A.1 Classification Phase

Take N realizations $x^{(N)} = \{x_1, x_2, \ldots, x_N\}$, $x_j \in X$ for $j = 1..N$ where X is a discrete random variable with probability space (Ω, A, P). The finite realization space, $\Omega = \{a_1, a_2, ..., a_M\}$ of X is discretized into M distinct sets. The sigma-field A consists of subsets of Ω which we take to be the power set of Ω such that every outcome on the realization space is also an element of A and thus has a probability associated with it. The measure P is called the probability measure, and $P(E)$ is the probability of the event E. The first N realizations are used to compute an empirical probability distribution.

$$\begin{aligned} v_{x^{(N)}}(a_j) &= \tfrac{1}{N}\sum_{i=1}^{N} 1_{a_j}(x_i), \qquad j = 1, \ldots, M \\ \text{where} \qquad 1_{a_j}(x_i) &= \left\{ \begin{array}{ll} 1 & \text{if } x_i = a_j \\ 0 & \text{if } x_i \neq a_j \end{array} \right\} \end{aligned} \tag{12}$$

The empirical distribution $v_1^{(N)}$ for the first N realizations is taken to represent the estimated probability law for the first distinct region. Subsequent sets of N readings $x_k^{(N)}$ and corresponding empirical distributions v_k are calculated using (12). Note that we drop the superscript N for notational convenience since N does not change with time. Each subsequent empirical distribution v_k is compared to the first empirical distribution v_1 to determine if v_k differs from v_1 in a statistically significant manner. A Minimum Description Length Test [16] is used to determine whether the two sequences estimated by v_k and v_1 came from the same probability law or if v_k constitutes

a distinct probability law different from v_1,

$$\frac{M-1}{N}\left[2\log\left(N+1\right)-\log\left(2N+1\right)\right] \begin{matrix} H_0 \\ > \\ < \\ H_1 \end{matrix} D\left(v_1 \parallel \mu_k\right)+D\left(v_k \parallel \mu_k\right) \tag{13}$$

where $\mu_k = \frac{1}{2}\left(v_1 + v_k\right)$ denotes the even mixture of the two compared distributions v_1 and v_k. The relative entropy or Kullback Leibler distance [17] between two probability distributions p and q is defined

$$D\left(p \parallel q\right) = \sum_{x \in X} p\left(x\right) \log \frac{p\left(x\right)}{q\left(x\right)} \tag{14}$$

Although $D\left(p \parallel q\right)$ is often called a distance, it is not a true metric because it is not symmetric nor does it satisfy the triangle inequality. The Kullback Leibler distance does posses many important mathematical properties such as $D\left(p \parallel q\right) \geq 0$ with equality only when $p = q$. Relative entropy is often used as measure of distance between two probability distributions. In (13), N represents the number of realizations or samples taken and M is the discretization of the realization space Ω. When hypothesis H_0 is satisfied, the measurements which correspond to v_1 and v_k are considered to be from the same probability law. Hypothesis H_1 is satisfied when v_k is significantly different such that measurements from v_k are governed by a different probability law than the measurements of v_1. During the classification phase, the Minimum Description Length test (13) is repeated for successive v_k until hypothesis H_1 is satisfied. Once this occurs v_k is assigned to v_2 , where v_2 represents the estimated probability law for the second distinct region, and the classification phase is completed.

A.2 Tracking Phase

After the classification phase is completed the two empirical distributions v_1 and v_2, represent probability laws governing two distinct regions of the environment. Using v_1 and v_2 the tracking phase determines the relative percentage of each distribution governing the current set of realizations.

Subsequent sets of realizations, $x_k^{(N)} = \{x_1, x_2, \ldots, x_N\}$, are taken and corresponding empirical distributions, v_k, are calculated using (12) as in the classification phase. The current distribution, v_k, can be represented as a mixture of the two probability laws found in the classification phase as $v_k = \pi_k v_1 + \left(1 - \pi_k\right) v_2$. Making use of the Kullback Leibler distance, the relative percentage, π_k, of the two distinct regions observed in the current empirical distribution is

$$\pi_k = \frac{D\left(v_k \parallel v_2\right) + D\left(v_2 \parallel v_1\right) - D\left(v_k \parallel v_1\right)}{D\left(v_1 \parallel v_2\right) + D\left(v_2 \parallel v_1\right)} \tag{15}$$

where π_k takes on values between 0 and 1 with extremes at $v_k = v_1$ and $v_k = v_2$, respectively. The relative percentage of observed regions π_k can be utilized to characterize the process boundary, which can be used in several applications.

B. Boundary Tracking

An application of this boundary detection technique, presented in [1], is the tracking of the boundary defined by the two regions of interest. Using π_k from (15), an error signal is defined as

$$\varepsilon_k \equiv \pi_k - 0.5 \tag{16}$$

which is used to maintain a $50-50$ mixture of the ambient and process distributions. A standard proportional-derivative yaw controller is implemented using the error signal to command angular velocity of the AUV,

$$\kappa_k = K_p \varepsilon_k + K_d \left(\varepsilon_k - \varepsilon_{k-1}\right) \tag{17}$$

Simulations of the boundary tracking algorithm were performed using the neutral tracer data from Section II. The neutral tracer and vehicle trajectory are shown in Figure 6. Despite the observed process being noisy and non-uniform the boundary tracking algorithm is able to maintain a path about the general boundary of the process.

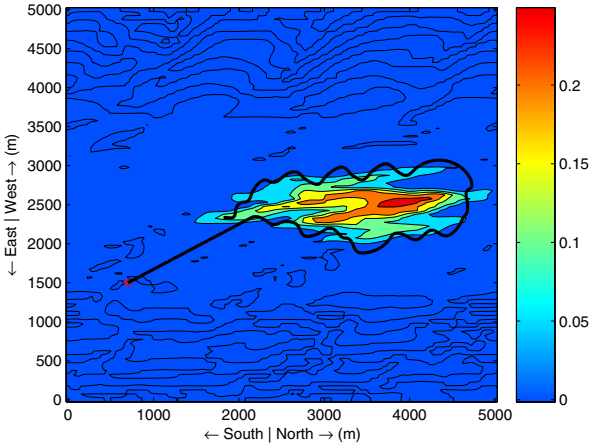

Fig. 6. Boundary tracking using control law (17).

C. Center of Mass Estimation

Another application resulting from the boundary detection technique in Section III-A is estimating the center of mass of a closed process. The AUV takes multiple cross section observations of the closed process, and while in the interior of the process it estimates the center of mass of the process using a weighted sum of measurements. As the AUV passes back on the process boundary,

it turns around and navigates toward the estimated center of mass. Once the AUV has reached the location of the current center of mass estimate the vehicle travels in a straight trajectory exiting the process before turning around and starting again.

The relative percentage of observed regions π_k is used with two threshold values to determine whether the AUV is inside or outside the neutral tracer patch being measured.

$$\begin{array}{ll} \pi_k < 0.2 & \textit{inside patch} \\ \pi_k > 0.8 & \textit{outside patch} \end{array} \tag{18}$$

When the AUV is inside the patch, the current position $r_k \in \mathbb{R}^2$, and a measurement of a neutral tracer patch $m_k \in \mathbb{R}$, are added to the current center of mass estimate

$$R_k = \frac{\sum_{k=1}^{m} r_k m_k}{\sum_{k=1}^{n} m_k} = \frac{\sum_{k=1}^{m} r_k m_k}{M_k} = \frac{R_{k-1}M_{k-1} + r_k m_k}{M_{k-1} + m_k} \tag{19}$$

where $R_k \in \mathbb{R}^2$ and $M_k \in \mathbb{R}$ are the center of mass position and total mass at time step k, respectively. A single measurement at time k is denoted by the pair (r_k, m_k). Only R and M are stored between time steps with the k^{th} measurement pair (r_k, m_k) updating the center of mass estimate according to (19). As the vehicle makes successive passes through the estimated center of mass, we observe through simulation that the center of mass estimate converges to the true center of mass.

Simulations of the center of mass estimation algorithm were performed using the same data set considered in section III-B. The vehicle path and center of mass estimate are shown in Figure 7. The white dot inside the process denotes the true center of mass calculated by sampling the entire domain at $50m$ intervals and calculating the weighted average. The dark blue line (center of mass estimate) begins in a straight line coincident to the initial vehicle trajectory. Once the vehicle makes its first turn the center of mass estimate is free to move in two dimensions. Note that the magnitude of the center of mass estimate in Figure 9 decreases as the center of mass estimate approaches the true center of mass in Figure 7.

Although the center of mass simulations were performed using a static data set, the algorithm can be extended to work with time varying data. However, using the center of mass estimation algorithm presented above for a time varying field will fail because over time the center of mass estimate will lag behind the true center of mass as obsolete measurements bias the center of mass estimate. One method to overcome this is if the old measurements decay with time so that new measurements carry more weight in the estimate.

Extending the center of mass estimation algorithm for use with multiple AUVs improves the convergence rate.

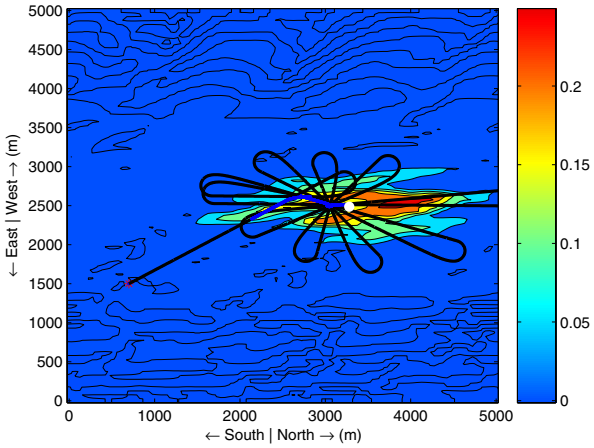

Fig. 7. Center of mass estimate and vehicle trajectory. The large blue line is the center of mass estimate while the thin black line is the vehicle course. The white dot is the true center of mass of the process.

Given a platoon of n vehicles, let (R_{i_k}, M_{i_k}) represent the center of mass estimate of the i^{th} vehicle in the platoon. When communication between one or more vehicles is available, their center of mass estimates, (R_{i_k}, M_{i_k}) are shared and each vehicle determines a global center of mass estimate

$$R_k = \frac{\sum_{i=1}^{n} R_{i_k} M_{i_k}}{\sum_{i=1}^{n} M_{i_k}} \tag{20}$$

Each vehicle can then base future path planning according to the global center of mass estimate (20) while still maintaining its own individual center of mass estimate. Because each vehicle maintains its own center of mass estimate which is independent of other vehicles, sharing estimates between vehicles simply replaces the previous estimate which vehicle i, has for vehicle j. A desirable consequence of this method is that no communications requirements are imposed on the vehicle platoon. Whenever vehicles communicate they will benefit from the additional information by making better path planning decisions. However, communication is not required for the platoon to function.

Initial studies were performed in which two vehicles estimated the center of mass of the neutral tracer data while sharing their respective center of mass estimates. Significant performance gains were achieved in the amount of time required to attain accurate center of mass estimates. Figure 8 shows two vehicles approaching the tracer from different sides of the process, as well as their combined center of mass estimate. Comparing the estimation errors in Figure 9 between the single and multiple vehicle simulations, shows almost a two fold decrease in the amount

of time required to reach equivalent estimate errors when using two vehicles.

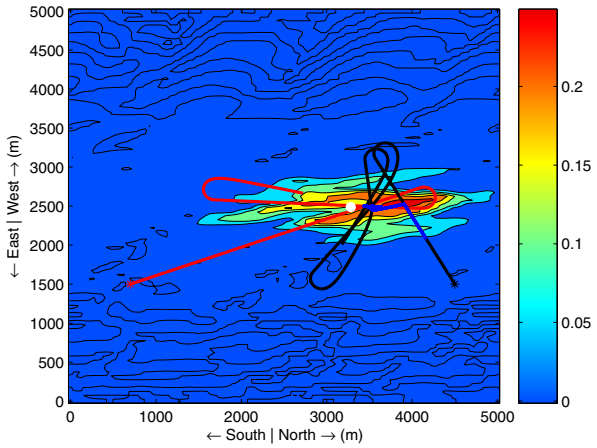

Fig. 8. Two vehicles estimating the center of mass of the neutral tracer. Each vehicle trajectory is denoted by a thin line. Their combined center of mass estimate is the dark blue line. The white dot is the true center of mass of the process.

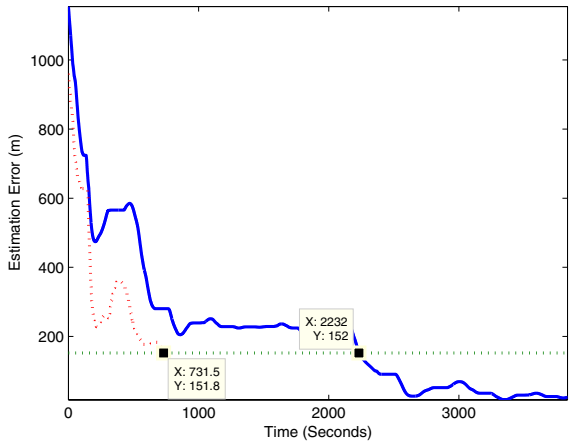

Fig. 9. Center of mass estimation error for single and multiple AUVs. The solid blue line depicts the estimation error for the single vehicle simulation while the dashed red line indicates the estimation error for two AUVs sharing their respective center of mass estimates. At 731 seconds the center of mass estimation error, when using two AUVs is that of the single vehicle simulation at 2232 seconds.

IV. Concluding Remarks

Two fundamentally different approaches for mapping and tracking marine processes have been presented. In the first parametric approach, parameters of an assumed process model are estimated using either an extended Kalman filter or nonlinear regression. Given measured data that closely matches the assumed model, this approach produces acceptable results. Selection of such a model remains an open question for small-scale turbulent natural phenomena. The second approach uses information theoretic techniques as an alternate method for mapping and tracking marine processes without the need for an accurate process model. Utilizing learned empirical probability distributions which represent statistically different process regions, little a priori knowledge of the environment is required. While this approach appears to work very well in our initial numerical experiments, their true utility cannot be determined until they are evaluated in the field. Additional concerns and corresponding open research questions center on the use of divergence as a measure of distance between distributions and the minimum description length test as a method for discriminating and classifying distributions. Other distance measures and classification methods are available in the literature, and several are the focus of our future work.

V. Appendix

A. Outline of Minimum Description Length Test

The Minimum Description Length Test between two empirical probability distributions presented in section III-A.1 was developed in [14] and [15]. An outline of this MDL test is given for reference. See [14] and [15] for details and further discussion.

The Minimum Description Length principle [16] states that the hypothesis that corresponds to the smallest complexity, or largest data compression, represents the best choice. According to this reasoning the choice between two hypothesis

$$\begin{array}{ll} H_0 : x_1^{(N)} \propto p_\mu^N & x_2^{(N)} \propto p_\mu^N \\ H_1 : x_1^{(N)} \propto p_{\mu_1}^N & x_2^{(N)} \propto p_{\mu_2}^N \end{array} \tag{21}$$

where μ, μ_1, and μ_2 are unknown probability distributions, is

$$\min_{H_i} I\left(x|H_i\right) \tag{22}$$

The stochastic complexity $I\left(x|H_i\right)$ can be approximated as

$$I\left(x|H_i\right) \approx -\log\left(p\left(x|H_i\right)\right) + L\left(H_i\right) \tag{23}$$

Where $p\left(x|H_i\right)$ is the probability of x given hypothesis H_i and $L\left(H_i\right)$ is the number of symbols required to describe the probability law selected for H_i. A result from type theory [18], relates the probability of obtaining the sequence $x^{(N)}$ governed by μ, to the type, $v_{x^{(N)}}$, of the sequence.

$$p_\mu\left(X = x^{(N)}\right) = \exp\left\{-N\left[H\left(v_x\right) + D\left(v_x||\mu\right)\right]\right\} \tag{24}$$

The Shannon entropy [19] denoted by $H\left(v_x\right)$, is a measure of the randomness or equivalently, the amount of information present in a distribution.

Evaluating (24) in (23) yields the following inequality

$$L(H_1) \underset{H_1}{\overset{H_0}{\gtrless}} N\left[D(v_1||\hat{\mu}) + D(v_2||\hat{\mu})\right] + L(H_0) \tag{25}$$

where $\hat{\mu}$, the estimate of μ, represents the empirical estimate of the mixture of the two types.

$$\hat{\mu} = \frac{1}{2}(v_1 + v_2) \tag{26}$$

The code length $L(H_i)$ represents the number of symbols required to describe sequences distributed according to μ, μ_1, and μ_2 under hypothesis H_i. Given that v_i is a rational number

$$v_i = \frac{n_i}{n} \text{ for } n_i \in \{0, ..., N\}, \text{ and } i \in \{0, ..., M\} \tag{27}$$

an upper bound on the set of all possible sequences of length N is defined as $(N+1)^M$ where M is the size of the alphabet. The upper bound can further be reduced to $(N+1)^{M-1}$ due to the fact that $\sum_{i=1}^{M} v_i = 1$. The maximum code length for a sequence of N realizations becomes

$$\begin{aligned} L\left(v^{(N)}\right) &= \log(N+1)^{M-1} \\ &= (M-1)\log(N+1) \end{aligned} \tag{28}$$

Computing $L(H_0)$ and $L(H_1)$ using (28) and substituting in (25) the desired result is obtained

$$\frac{(M-1)}{N}\left[2\log(N+1) - \log(2N+1)\right] \underset{H_1}{\overset{H_0}{\gtrless}} D(v_1||\hat{\mu}) + D(v_2||\hat{\mu}) \tag{29}$$

VI. Acknowledgment

The authors gratefully acknowledge the support of the National Science Foundation via grants IIS-0238092 and OCE-9354810, and the Office of Naval Research via grants N00014-03-1-0444 and N00014-05-1-0780.

References

[1] C. Barat and M.J. Rendas, "Benthic boundary tracking using a profiler sonar," in *Proc. IEEE/RSJ Int. Conf. Intelligent Robots and Systems*, Oct 2003, vol. 1, pp. 830– 835.

[2] C. J. Cannell, D. J. Stilwell, and J. A. Austin, "A simulation tool to support the development of adaptive sampling algorithms for multiple autonomous underwater vehicles," in *Proc. of the IEEE Workshop on Autonomous Underwater Vehicles*, Sebasco Estates, ME, 2004.

[3] Vassilios N. Christopoulos and Stergios I. Roumeliotis, "Adaptive sensing for instantaneous gas release parameter estimation," Tech Report 2004-0001, Center for Distributed Robotics, University of Minnesota, Minneapolis, MN, June 2004.

[4] Aleksandar Jeremic and Arye Nehorai, "Landmine detection and localization using chemical sensor array processingn," *IEEE Trans. Signal Processing*, vol. 48, no. 5, pp. 1295–1305, May 2000.

[5] Dimitri Zarzhitsky, Diana Spears, David Thayer, and William Spears, "Agent-based chemical plume tracing using fluid dynamics," in *Lecture Notes in Computer Science, Vol. 2338*. Springer-Verlag, 2004.

[6] D.O. Popa, A.C. Sanderson, R.J. Komerska, S.S. Mupparapu, D.R. Blidberg, and S.G. Chappel, "Adaptive sampling algorithms for multiple autonomous underwater vehicles," in *Proc. IEEE Workshop on Autonomous Underwater Vehicles*, Sebasco Estates, ME, June 2005.

[7] Adam T. Hayes, Alcherio Martinoli, and Rodney M. Goodman, "Swarm robotic odor localization: Off-line optimization and validation with real robots," *Robotica*, vol. 21, pp. 427–441, 2003.

[8] Frank W. Grasso, Thomas R. Consi, David C. Mountain, and Jelle Atema, "Biomemetic robot lobster performs chemoorientation in turbulence using a pair of spatially separated sensors," *Robotics and Autonomous Systems*, vol. 30, pp. 115–131, 2000.

[9] J. A. Farrell, S. Pang, and W. Li, "Plume mapping via hidden markov methods," *IEEE Trans. Syst., Man, Cybern. B*, vol. 33, no. 6, pp. 850 – 863, 2003.

[10] J. A. Farrell, W. Li, S. Pang, and R. Arrieta, "Chemical plume tracing experimental results with a REMUS AUV," in *Proc. IEEE/MTS OCEANS*, 2003, pp. 962–968.

[11] Kalman, *Kalman Filtering: Theory and Application*, IEEE Press, 1985.

[12] R. S. Bucy and P. D. Joseph, *Fitering for Stochastic Processes with Applications to Guidance*, Wiley, New York, 1968.

[13] G.A.F Seber and C.J. Wild, *Nonlinear Regression*, John Wiley and Sons, 1989.

[14] Albert Tenas, *Unsupervised Segmentation of Images Based on the Kullback Distance*, Dissertation, Laboratoire d'Informatique, Signaux et Systemes de Sophia Antipolis, UPC Barcelona, June 2001.

[15] Albert Tenas, Maria-Joo Rendas, and Jean-Pierre Folcher, "Image segmentation by unsupervised adaptive clustering in the distribution space for auv guidance along sea-bed boundaries using vision," Honolul, Hawaii, November 2001.

[16] Jorma Rissanen, *Stochastic complexity in statistical inquiry*, World Scientific Pub Co Inc, Nov 1989.

[17] S. Kullback, *Information Theory and Statistics*, John Wiley and Sons, 1959.

[18] Imre Csiszar, "The method of types," in *IEEE Transactions on Information Theory*, vol. 44, pp. 2505–2523. IEEE Press, Oct 1998.

[19] C.E. Shannon, "A mathematical theory of communication," Tech. Rep., Bell Systems, 1948.